Constructed Facilities Laboratory Department of Civil, Construction, and Environmental Engineering

Technical Report
No. IS-06-02

DESIGN GUIDELINES FOR THE USE OF HM STRIPS:

STRENGTHENING OF STEEL CONCRETE COMPOSITE BRIDGES WITH HIGH MODULUS CARBON FIBER REINFORCED POLYMER (CFRP) STRIPS

David Schnerch
Mina Dawood
Dr. Sami Rizkalla

June 2007

Constructed Facilities Laboratory

2414 Campus Shore Drive

North Carolina State University
Raleigh, NC 27695-7533
Tel: (919) 513-1733
Fax: (919) 513-1765
Email: cfl@ncsu.edu

STRENGTHENING OF STEEL-CONCRETE COMPOSITE BRIDGES WITH HIGH MODULUS CARBON FIBER REINFORCED POLYMER (CFRP) STRIPS

David Schnerch
Mina Dawood
Dr. Sami Rizkalla

1. INTRODUCTION

Proper installation and design of high modulus CFRP strips is essential in ensuring both the long-term performance of the system and that the behavior of the system matches the intentions of the designer. A certain level of care and expertise is required to ensure that these goals are met. These installation and design guidelines represent the current best practice available based on a thorough review of the literature and considerable personal experience in bonding CFRP materials to steel surfaces.

2. HIGH MODULUS CFRP STRENGTHENING SYSTEM

2.1 High Modulus Strips

High Modulus (HM) carbon fiber reinforced polymer strips are a pultruded laminate with sufficient strength and stiffness to strengthen steel structures, as shown in Figure 1. The carbon fibers used in these strips are the DIALEADK63712 high modulus pitch based carbon fibers produced by Mitsubishi Chemical Functional Products, Inc. (MCFP). These strips may be bonded onto steel structures as an external reinforcement using an epoxy adhesive, offering an efficient method for increasing structural stiffness. HM strips, the commercial product "e-PLATE HM"

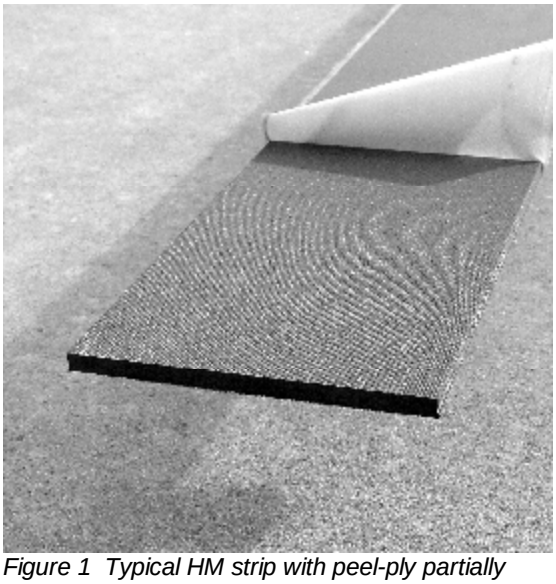

Figure 1 Typical HM strip with peel-ply partially removed

by MCFP, have a tensile modulus that is two times that of steel as listed in Table 1. This provides users with the ability to improve structural stiffness, lower deflections while minimizing the thickness of the CFRP required, providing designers and installers an economical solution for steel structural upgrades.

Table 1 Material properties of HM strips

	Minimum value		Mean value	
Tensile strength	1200 MPa	174 ksi	1500 MPa	218 ksi
Tensile modulus	420 GPa	61,000 ksi	450 GPa	65,000 ksi
Ultimate elongation	0.27 %		0.34 %	
Density	-		1.82 g/cm^3	
Fiber volume fraction	-		71 %	
Glass transition temperature	80 °C	176 °F	100 °C	212 °F

2.2 Adhesive

Six different adhesives were evaluated for use in bonding the HM strips to steel using scaled steel flexural specimens (Schnerch and Rizkalla, 2004). Of the adhesives studied, SP Systems Spabond 345 epoxy adhesive resulted in the shortest development length of the products studied. Based on its level of performance in these preliminary trials, and subsequent performance in strengthening large-scale steel-concrete composite beams, Spabond 345 is recommended for use with the HM strips.

3. INSTALLATION RECOMMENDATIONS

3.1 Introduction

Bonded joints are an effective way to join two different adherends, since the resulting stress concentrations of the joint are lower than for bolted connections. This is particularly important in using CFRP materials, since the strength of the material perpendicular to the fiber direction is relatively low. At all times the designer must understand the importance of the requirements for achieving a good bond, firstly through direct contact between the adhesive and the substrate, and secondly through the removal of weak layers or contamination at the interface (Hutchinson, 1987).

Installation of HM strips requires a multi-step approach, beginning with the delivery of the strips to the site. Careful planning and consideration of all the steps is important from the outset since several of the steps are time critical. The HM strips should be cut to length and have their ends detailed prior to surface preparation of the steel. Once all the surfaces are prepared, the adhesive must be thoroughly mixed, applied to the bonding surfaces and clamped within the pot-life of the adhesive. Finally, proper protection of the HM strips must be conducted to prevent against environmental degradation through processes of galvanic corrosion and ultraviolet exposure.

3.2 Shipping and Storage

The HM strips should be shipped in a rigid container that prevents impacts from damaging the strips. Upon arrival at the site, all the HM strips should be inspected to ensure there are no cracks, notches or out-of-straightness of the strips. If replacement material is required, it should be procured before the surface preparation of the steel takes place. The HM strips and the adhesive should be stored in a cool, ventilated place, avoiding direct sunlight. Avoid freezing and drying of the resin. Store resins in a tightly closed containers to prevent moisture contamination.

3.3 Pre-Bonding Fabrication

Before commencing the surface preparation, the HM strips should be cut to length and have their ends detailed in accordance with the design for the adhesive joint. HM strips may be cut to length by hand using a fine tooth saw blade and a miter box, keeping in mind that a dust mask should be worn to ensure that the dust particles are not inhaled. The FRP material should never be drilled and it is recommended that cutting with power tools be avoided due to the large amount of dust that this creates.

The design of the adhesive joint is governed by stresses that are critical near the ends of the HM strip. Several researchers have found significant performance increases can be achieved by tapering the thickness of the CFRP material at the edges, while correspondingly increasing the adhesive thickness (Allan ***et al.***, 1988,

and Price and Moulds, 1991). By detailing the ends of the HM strips to have this reverse taper, as shown in Figure 2, considerable performance enhancement can be achieved for both static and fatigue behavior.

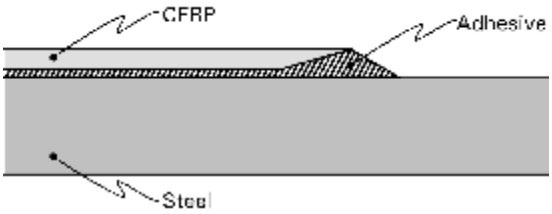

Figure 2 Configuration of reverse tapered joint

As the length of the taper increases, so does the reduction in the stress concentration at the edge of the HM strip. The effectiveness of the tapering the HM strips must be weighed against the practicality of providing a long taper. It has been found that a taper of 10-20 degrees is easily fabricated with a mechanical sander and sanding in the direction of the fiber, as shown in Figure 3, while maintaining much of the performance enhancement of a longer taper. Thus, a recommended taper would have a taper length that is three to five times the strip thickness for situations where a reduction in the bond stresses at the end of the strip is determined to be necessary.

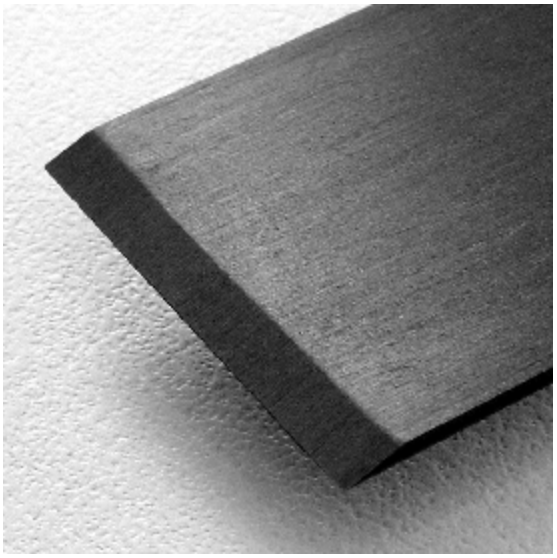

Figure 3 HM strip with a 20 degree taper at the end

3.4 Surface Preparation of the Steel Surfaces

Surface preparation is fundamental in ensuring adequate bond and involves cleaning, followed by the removal of weak layers and then recleaning (Mays and Hutchinson, 1992). Surface preparation of the steel must be undertaken to enhance the formation of chemical bonds between the steel and the adhesive. This requires a chemically active surface that is free from contaminants and laitance.

The surface of the steel should be largely flat, since the HM strips will not conform to any surface irregularities, such that these irregularities could result in an uneven bond line or voids between the CFRP material and the steel. Alternatively, for highly irregular surfaces, application by wet lay-up of CFRP sheets is recommended where a moderate strength increase is desired and the number of

plys required is reasonable, since this process allows the sheets to conform to the surface configuration of the steel.

The most effective way of achieving a chemically active surface is by grit blasting (Sykes, 1982, Hutchinson, 1987, and Hollaway and Cadei ***et al***., 2004). Grit blasting procedures, using angular grit remove the inactive oxide and hydroxide layers on the surface of the steel by cutting and deformation of the base material. Sanding or grinding the steel should be avoided since this process leaves the surface of the steel smooth and does not effectively remove the contaminants, but can redistribute these contaminants into the surface. Preparation by sanding has been shown to results in lower bond strengths than grit blasting (Parker, 1994).

Before grit blasting, the steel surface should be completely free from oils or other contaminants. Acetone, or a solvent suitable to remove the particular contaminant, should be used to remove these contaminants. This is especially critical when the grit to be used will be recycled, to ensure that the grit does not become contaminated with substances that are detrimental to the bond performance. Requirements for the physical properties of the grit and its size are listed in Table 2. In general, the grit should be angular, hard, properly graded, dry, and free of contaminants.

Table 2 Grit requirements for surface preparation of the steel

Property	Minimum value
Specific gravity	2.65
Moh's hardness	6.5
Shape	angular

US standard screen	Percent retained per sieve
16	0.4
20	11.3
30	43.0
40	33.9
50	8.5
pan	2.9

Grit blasting should be completed until a "white metal" surface, as shown in Figure 4, with a rough texture is achieved. Particular attention should be given to the steel near to where the ends of the strip will be bonded, since the stresses in the adhesive will be highest in this region. After grit blasting, any surface dust should be removed by brushing, vacuuming or blowing with a clean uncontaminated air supply. A final solvent cleaning after grit blasting may be completed, but extreme care must be taken to ensure that liberal amounts of solvent are used, such that contaminants that are brought into solution drip or flow off the structure and are not merely redistributed when the solvent evaporates. Taking into account probable environmental constraints, the best method is likely to be by brushing and vacuuming.

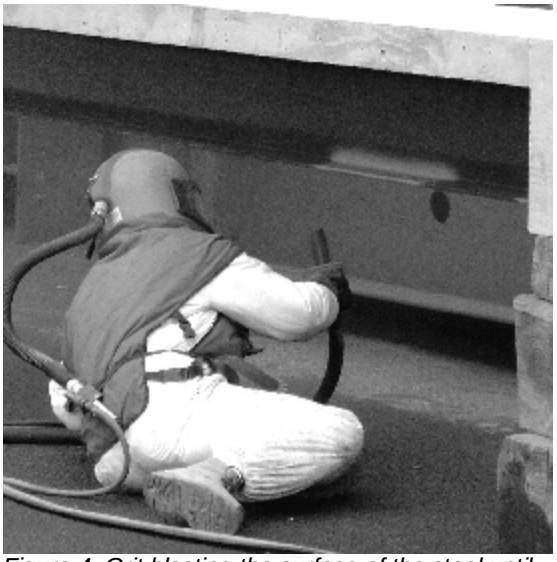

Figure 4 Grit blasting the surface of the steel until a "white metal" surface is achieved

Application of the adhesion promoter or HM strip should take place as soon as possible after the surface preparation to ensure that the surface is minimally oxidized before the adhesive is applied. As a guideline, no more than 24 hours should occur between the time of sandblasting and the time the surface is coated with the adhesion promoter or adhesive. Minimizing this interval is preferable, and Cadei ***et al.*** (2004) recommends that application of the primer coat or adhesive should take place no more than two hours after grit blasting the steel. In conditions of moderate humidity, immediate adhesive application following grit blasting would be highly recommended. Grit blasting should be avoided in conditions of high humidity.

3.5 Surface Preparation of the CFRP Surface

For the CFRP surface, it is usually desirable that the HM strip be fabricated with a peel-ply on one or both sides of the strip. This peel-ply is an easily removable layer that is weakly attached to the surface of the strip during its manufacture, and

protects the surface from contamination. The peel-ply should be left on the HM strip until just before bonding, to prevent contamination of the surface. It is recommended that all traces of the peel ply be removed from the surface of the HM strip. Touching the strip on the side to be bonded should be avoided since contaminants from the hands may affect the bond.

If a peel-ply is not available for the HM strips, it is necessary to follow the recommendations of Hollaway and Cadei (2002) in preparing the surface of the CFRP. The strips should be lightly abraded on the side to be bonded with sandpaper and cleaned with a solvent, such as methanol.

3.6 Use of Adhesion Promoters

For application in a moist environment, the use of silane adhesion promoters on the steel surface is recommended. These adhesion promoters have been shown to increase the durability of steel-epoxy bonds without affecting the bond strength (McKnight ***et al***., 1994). They have also previously been used successfully in repairing aluminums structures with CFRP materials (Hutchinson, 1987). Adhesion promoters work by developing stronger bonds to the steel surface than epoxy is able to achieve. These bonds reduce the primary mechanism for strength reduction in moist environments: interfacial attack by the moisture, which is energetically attracted to the steel surface. This moisture can adsorb onto the surface of the steel, displacing the secondary bonds between the adhesive and the substrate (Hashim, 1999). Compounding this effect is that moisture ingress occurs at the edges of a joint, where the stresses are the highest.

Due to the excellent lab performance of adhesion promoters, they have been used in field applications, such as the strengthening of bridge 1-704, which carries southbound traffic on Interstate 95 in Delaware (Miller ***et al***., 2001). Some adhesives incorporate silanes into their formulation, but naval applications have indicated that this is less effective than a separate silane layer (Allan ***et al***., 1988). The Z-6040 silane produced by Dow-Corning was used as a primer in conjunction with the Spabond 345 epoxy resin produced by SP Systems to strengthen a steel-concrete composite beam which was subsequently tested in fatigue to 3 million

cycles (Dawood, 2005). Based on the results of this experimental program the use of the adhesion promoter did not affect the fatigue behavior of the strengthening system.

3.7 Application of the Adhesive and Installation

A trowel with a v-notch should be used to spread the adhesive to ensure a uniform coating is achieved. A 4.8 mm (3/16 inch) notch resulted in an adhesive thickness of 0.6 mm to 1.2 mm that was used by Schnerch and Rizkalla (2004) with the Spabond 345 epoxy resin produced by SP Systems. Thin bond lines result in higher shear and normal stresses in the adhesive at the ends of the strip, but as the thickness of the bond line increases, so does the bond line porosity and this decreases the shear and peel strengths markedly over the life span of the structure. However, considering the potential for galvanic corrosion, it is recommended that the bond line have sufficient thickness to ensure that a layer of adhesive separates the steel and the CFRP along the entire bonded area. Guidelines have indicated that metal and FRP joints in general should have a target thickness of 0.5-2.0 mm (Institution of Structural Engineers, 1999). For the specific case of steel-concrete composite beams strengthened with HM strips, adhesive thicknesses of 0.1-1.0 mm have been successfully used for beams that were tested in fatigue (Dawood, 2005). The 1.0 mm adhesive thickness was achieved by thoroughly mixing 0.8–1.2 mm diameter E-glass spacer beads into the adhesive before applying the adhesive to the CFRP strips. The behavior of the tested beams was not affected by the adhesive thickness throughout a 3 million cycle loading course.

The epoxy may be applied directly to the surface of the HM strip, however for highly irregular surfaces it is recommended that the adhesive should be applied to both surfaces. The final thickness of the adhesive layer should be within the guidelines established by the designer.

3.8 Installation, Clamping and Coating

The strip, with adhesive on one side, should be pressed into the steel from one end, and gradually worked towards the other edge to allow air to escape as the adhesive is pressed in. Multiple plys may be installed, but the efficiency of the

strengthening is greatly reduced as the number of plies increases due to the shear-lag effect.

A laminate roller should be used to ensure that maximum contact is obtained between the HM strips, the adhesive and the steel substrate. Rolling should occur from the center of the strip and worked outwards to ensure as much air as possible is removed from the bond line. Care must be taken to ensure that too much adhesive is not squeezed out of the ends of the strip. In this region, it is particularly critical to maintain a bond line that is consistent with the rest of the strip. It is preferable if the adhesive thickness at the ends of the strip is slightly thicker, to reduce the adhesive stresses at the strip ends. Once the HM strip, the adhesive and the steel surface are completely in contact, clamping of the strip to the steel should be completed within the pot-life of the adhesive, as shown in Figure 5.

Figure 5 Clamping the HM strips within the pot-life of the adhesive

If the length of the member being strengthened is longer than the available length of HM strips, then splices may be used to allow force transfer between two or more separate strips. Splice locations should be away from the portion of the member subjected to the highest bending moment. The necessary length of the splice will depend on the adhesive being used, the thickness of the HM strip and the material properties of the strip itself. In one study, a steel-concrete composite beam was strengthened with HM strips with a tensile modulus of 230 GPa and a thickness of 3.2 mm (Schnerch and Rizkalla, 2004). The tested beam incorporated a 400 mm long splice joint, using the same type of CFRP material, which was located at approximately the quarter span of the beam. The test results indicate that the

splice joint adequately transferred the stress in the CFRP until rupture of the strips occurred away from the splice location.

Temperature changes during the lifespan of the strengthening system can induce stresses in the adhesive, the CFRP materials and the steel beam which should be carefully considered during by the designer. Steel expands when heated, whereas the CFRP material can be expected to have a very small or negative coefficient of thermal expansion. For the same reason, heat cured adhesives must be carefully considered to account for the stresses induced during the heated cure and the subsequent removal of heat. Temperature changes can occur due to daily and seasonal variations in the ambient air temperature, due to direct exposure to sunlight or shade or possibly due to accelerated curing of the adhesive at high temperatures among other causes. In any case, the designer should carefully consider the effect of these thermal variations and ensure that the induced stresses are acceptable.

Prevention of galvanic corrosion is a particular requirement for design. Three conditions are necessary for galvanic corrosion to occur (Francis, 2000). An electrolyte (such as salt water) must bridge the two materials, there must be direct electrical connection between the materials and there must be a sustained cathodic reaction on the carbon fiber. Controlling any one of these conditions is sufficient to ensure that no galvanic current is generated.

Providing a consistent thickness of adhesive between the steel and the FRP is the first defence against galvanic corrosion. A second, necessary, step is a top coating of epoxy or other sealant to ensure moisture is excluded from the bond line. In the presence of repeated wetting, the bond line can absorb moisture together with any electrolytic ions present in the environment. These can allow electrical currents to be established, leading to the formation of galvanic corrosion. By excluding moisture from the bond line, no electrolytical solutions can bridge between the steel and the CFRP material, and also the resistance to electric current of the adhesive layer is ensured.

Glass fiber layers within the bond line have often been proposed to eliminate the potential for galvanic corrosion. However, epoxy is inherently hydrophilic (Hand ***et al***., 1991) and electrolytic ions may be leached out of the glass fiber in the presence of moisture (Miriyala ***et al***., 1993). This process has been found by Miriyala to lead to blistering of CFRP materials that included glass fiber due to concentration gradients that favor the movement of moisture into the joint.

Lastly, proper drainage must be ensured to minimize the accumulation of condensation and rainwater. One such case where this may occur is if the HM strips were used on the top surface of the tension flange. Particular care would need to be taken to ensure that water and debris does not collect between the web and the HM strip.

4. DESIGN FOR FLEXURE

4.1 Introduction

As noted by Buyukozturk ***et al***. (2004) there are four potential failure modes for a steel beam strengthened with CFRP materials. These are failure by rupture of the FRP material, by debonding of the FRP material, buckling of the compression flange or shear failure of the web. For steel-concrete composite beams, crushing of the concrete in compression must also be considered. Of particular interest in these guidelines, are the failure modes by FRP rupture and FRP debonding. The remaining failure modes are failure modes for unstrengthened steel beams and unstrengthened steel-concrete composite beams, therefore are not dealt with here, but must be considered for any design. To prevent these failure modes, standard rational analysis methods must be employed, considering the effect of the FRP material in increasing the load carried by the beam at failure.

Installation of high modulus CFRP materials can increase the elastic stiffness of a steel beam and decrease the elastic strain at the tension flange of the beam as compared to an unstrengthened beam at the same load level. Due to these two effects, the live load capacity of a steel beam can be increased using externally bonded CFRP materials. To determine the allowable increase in the live load level for a strengthened beam, it is not sufficient to consider the ultimate capacity of the

strengthened beam only. Rather, to prevent failure of the strengthened beam due to fatigue of the steel at the increased load level, it is also important to limit the stress range at the tension flange of the steel beam.

4.2 Design Philosophy

The allowable increase of live load for a steel-concrete composite beam strengthened with HM CFRP materials should be selected to satisfy three conditions. These three conditions are shown in Figure 6 with respect to the moment-curvature response of a typical steel-concrete composite beam section strengthened with HM CFRP materials. Due to the presence of the additional layer of HM CFRP material, the yield moment of the strengthened beam, $M_{Y,S}$, is greater than yield moment of the unstrengthened beam, $M_{Y,US}$. The yield strength of the strengthened and unstrengthened beams, are defined as the moment corresponding to yielding of the extreme fiber of the tension flange of the steel beam in both cases. To ensure that the strengthened member remains elastic, the total applied moment acting on the strengthened beam under service loading conditions, including the effect of dead load, M_D, and the increased live load, M_L, should not exceed 60 percent of the increased yield moment of the strengthened beam. To satisfy the strength requirements, the total factored moment based on the appropriate dead load and live load factors, α_D and α_L respectively, should not exceed the ultimate moment capacity of the strengthened beam, $M_{U,S}$. The ultimate moment capacity of the strengthened section should be calculated based on the calculated nominal capacity while applying a suitable reduction factor to ensure the reliability of the strengthened girder. Also, to ensure that the structure remains safe in the case of total loss of the strengthening system, the total applied moment, including the effect of dead load and the increased live load should not exceed the residual nominal moment capacity of the unstrengthened beam, $M_{n,US}$. A limited fatigue study demonstrated that the HM CFRP strengthening system can sustain an increase of the live load level which induced a stress range in the tension flange of the steel beam of 30 percent of the yield strength of the steel (Dawood, 2005). The fatigue durability of two strengthened beams tested at this stress range was

comparable to that of a similar unstrengthened beam tested using the same stress range.

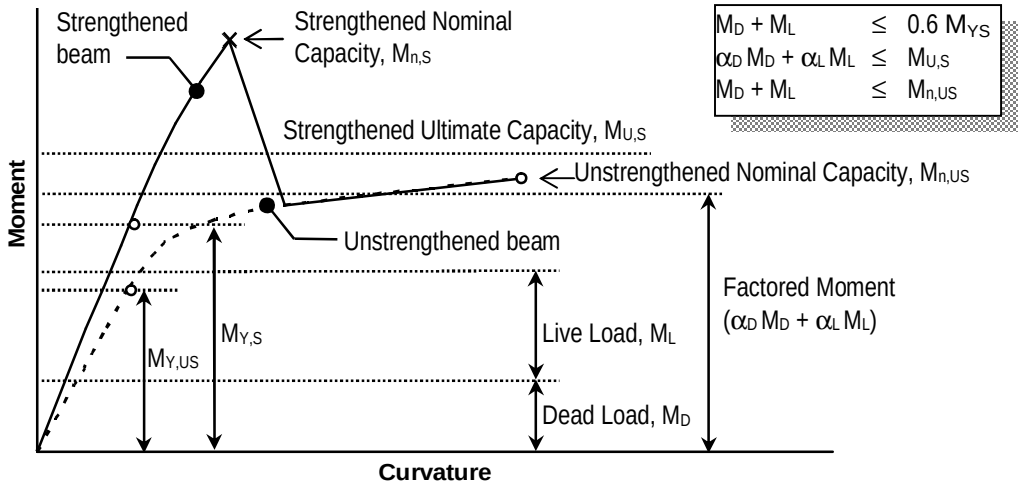

Figure 6 Load levels and moment-curvature behavior for a strengthened beam

4.3 Design Procedure

A moment-curvature procedure that was previously developed for prestressed concrete beams was adapted to predict the flexural behavior and failure mode of beams strengthened using HM CFRP strips (Mattock, 1979). This analysis is based on the cross-sectional geometry as well as the stress-strain behavior of the constituent materials using the principal of strain compatibility. The analysis procedure is summarized in this section. Schnerch (2005) and Dawood (2005) present a more detailed discussion of the analysis.

The moment-curvature behavior of a given cross-section is determined based on the strain at the top level of the compression flange as shown in Figure 7 together with an assumed neutral axis depth. This strain is subsequently increased to determine the next increment of curvature. The cross-section is broken down into levels corresponding to the concrete deck, the longitudinal steel reinforcement of the concrete deck, the flanges and web of the steel beam, and the HM CFRP strips at the bottom of the cross-section. The strain profile can be determined based on compatibility of strains using Equation (1) as illustrated in Figure 7. From the strain profile and the constitutive relationships of the materials, the corresponding stress profile for the beam can be established. Integration of the stress profile

using Equation (2) provides the resultant forces of the different components of the cross-section. For example, for the concrete deck, the strain, and corresponding resultant force can be determined as:

$$e_{c,x} = f\mathrm{x} \qquad \text{Equation (1)}$$

$$\mathrm{F_c} = \mathrm{b_c} \int_{c-t_c}^{c} \mathrm{f_c}(\mathrm{x})\mathrm{dx} \qquad \text{Equation (2)}$$

where

$\varepsilon_{c,x}$ = strain in the concrete deck at a distance x from the neutral axis

f = curvature of the section

x = distance above the neutral axis

F_c = resultant force in the concrete deck

b_c = width of the concrete deck

c = neutral axis depth

t_c = thickness of the concrete deck

$f_c(x)$ = stress in the concrete deck at a distance x from the neutral axis, defined by the constitutive relationship of the concrete

The critical strain for an unstrengthened beam will typically be the ultimate strain of the concrete deck slab. For the strengthened beam, this strain must be considered, but the ultimate strain of the HM strip is likely to govern the ultimate capacity of the member. Since the ultimate strain of the HM strip is typically reached well before the ultimate strain of the concrete, the equivalent rectangular stress block should not be used. The moment curvature analysis should be conducted using a non-linear constitutive model for the concrete such as that presented by Collins and Mitchell (1997) and used later in the Appendix of this guideline.

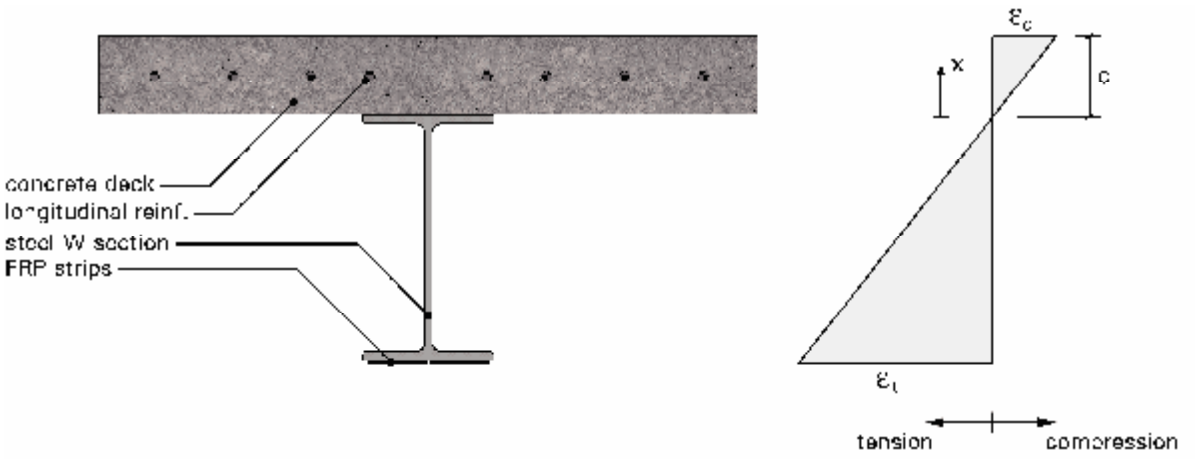

Figure 7 Assumed strain profile for steel-concrete composite beam strengthened with HM strips

To achieve horizontal equilibrium, the initially assumed neutral axis depth may be varied. Once horizontal force equilibrium is achieved, the locations of the resultant forces are necessary to determine the moment capacity of the section. These can be calculated by multiplying the term within the integral of Equation (2) by the distance from the neutral axis, x, and re-evaluating the integral.

This procedure can be easily implemented using commercially available computer software, such that the integrals can be evaluated numerically and the iteration procedure can be implemented automatically. Using this technique, any point or series of points on the nominal moment-curvature relationship of a strengthened section can be obtained. The moment-curvature diagram can be used with the moment-area method to obtain the expected load-deflection behavior for a given beam and loading configuration.

While the nominal behavior of the member can be used to predict the behavior under service loading conditions, the design ultimate capacity should incorporate suitable reduction factors to ensure that the member remains safe. These reduction factors should account for the uncertainty of the HM CFRP material properties and should take into consideration the sudden, brittle failure which is typical of most HM CFRP strengthened steel-concrete composite beams. This guideline has adopted the approach outlined in ACI 440.2R-02 for the calculation of the ultimate

capacity of concrete beams strengthened with externally bonded FRP materials. However, the approach has been modified to account for the inherent difference between the behavior of steel beams and concrete beams.

To account for the statistical uncertainty of the measured ultimate capacity of the HM CFRP materials, the mean strength of the CFRP reported by the manufacturer, $\bar{f}_{FRP,u}$, should not be used directly in calculating the ultimate capacity of the strengthened section. Rather, the average ultimate strength of the FRP should be reduced by 3 times the standard deviation, σ, as in Equation (3) (ACI 440.2R, 2002).

$$f^{*}_{FRP,u} = \bar{f}_{FRP,u} - 3s \qquad \text{Equation (3)}$$

To account for possible environmental degradation of the CFRP materials throughout the lifetime of the strengthening, ACI 440.2R-02 recommends the use of an environmental reduction factor, C_E. For carbon fiber materials subjected to exterior exposure, which is typical for most bridge structures, a value of C_E of 0.85 should be used. Therefore, the design strength of the HM CFRP material can be calculated as

$$f_{FRP,u} = C_E f^{*}_{FRP,u} \qquad \text{Equation (4)}$$

The design ultimate strain of the CFRP material, $\varepsilon_{FRP,u}$ can be calculated by dividing the calculated design strength of the CFRP by the average elastic modulus, E_{FRP}, reported by the manufacturer.

The nominal moment capacity of the strengthened member, $M_{n,S}$, should be calculated using the proposed moment-curvature procedure and the design strength and ultimate strain of the CFRP. The nominal capacity of a steel-concrete composite beam strengthened with high modulus CFRP materials is typically governed by rupture of the CFRP materials. This type of failure occurs in a sudden, brittle manner without significant warning. To account for the brittle nature of failure, a strength reduction factor, ϕ, of 0.75 is recommended. This reduction factor is consistent with the reduction used in the AISC LRFD

Specification for rupture type limit states. The design ultimate capacity of the strengthened beam, $M_{U,S}$ should be calculated as $\phi M_{n,S}$.

5. DESIGN FOR BOND

5.1 Introduction

The preceding analysis was based on the cross-section of the member alone, and assumed that the bond between the steel and the HM FRP material is perfect. While this assumption is sufficient to predict the flexural behavior of the HM FRP strengthened member up to the ultimate tensile strength of the HM FRP material, a premature debonding failure will result in the ultimate strength not being reached. Furthermore, since a debonding failure is typically sudden and without warning, considerable care must be taken to avoid its occurrence. As such, the shear and normal, or peeling stresses, need to be considered for each particular strengthening configuration.

An elastic stress-based analysis is recommended for the design. Although, an elastic approach may neglect reserve capacity in the adhesive after yielding of the adhesive, it is desirable to have yielding of the section occur before the adhesive becomes inelastic since yielding of the member is more visually apparent then any non-linear behavior of the adhesive and steps can be taken to address the overloading of the structure, if any. It has further been recommended that the maximum bond stresses in an adhesive joint should not exceed 20-30 percent of the ultimate strength of the adhesive under repeated fatigue loading conditions (Cadei et al., 2004). Designing a joint beyond its elastic strength may also result in poor creep performance.

An analytical procedure was developed for determining the bond stresses. This procedure allows the analysis of beams with bonded FRP strips to the tension side of the beam. The analysis includes the effect of the applied loading, the thermal effects resulting from differing coefficients of thermal expansion, as well as any prestressing applied to the FRP strip before bonding. Thermal effects should be considered for any structure that is subjected to thermal changes. More details

regarding the analysis, in addition to techniques to reduce the stresses at the ends of the HM strips may be found in Schnerch (2005).

5.2 Design Philosophy

The bond stresses arise from both shear stresses and normal or peeling stresses that are a result of the transfer of stresses from the beam to the bonded HM strips. As indicated by Cadei ***et al***. (2004), the strength of the bond must be determined empirically since this strength depends not only upon the properties of the substrates and adhesives, but also upon the degree of surface preparation that is expected. The characteristic strength of an adhesive system can be established using small scale single or double lap shear coupon tests. The test coupons should be prepared using the same materials, surface preparation techniques and application techniques as will be used for the strengthening project to ensure that the coupon test results are representative of the expected behavior. The maximum shear stress, τ, and normal stress, σ, can be determined from these preliminary tests using well established bond models such as those outlined for the case of double-lap shear specimens (Hart-Smith, 1980). Typically, the maximum shear and normal stresses are coincident along the length of the adhesive joint. These stresses can then be used to determine the maximum principal stress, σ_p, of the adhesive or interface using the equation,

$$s_p = \frac{s}{2} + \sqrt{\left(\frac{s}{2}\right)^2 + t^2} \leq s_c \qquad \text{Equation (5)}$$

where σ is the maximum normal stress and τ is the maximum shear stress of the joint. This characteristic strength, σ_c, represents the strength that should be used for design of the actual beam including any safety factors. Safety factors have been proposed for the joining of FRP materials that take into account the uncertainties in preparing an adhesive joint as well as the changes in material properties over time, as indicated in Table 3 (Institute of Structural Engineers, 1999). The overall safety factor for the joint is the product of the individual partial safety factors.

Table 3 Recommended values for partial safety factors for adhesive joints, adapted from Institution of Structural Engineers (1999)

	Partial Safety Factor
Source of the adhesive properties	γ_{m1}
- typical or textbook values	1.5
- values obtained by testing	1.25
Method of adhesive application	γ_{m2}
- manual application, no adhesive thickness control	1.5
- manual application, adhesive thickness controlled	1.25
- established application procedure with repeatable and controlled process parameters	1.0
Type of loading	γ_{m3}
- long-term	1.5
- short-term	1.0
Environmental conditions	γ_{m4}
- service conditions outside test conditions	2.0
- adhesive properties determined for service conditions	1.0
Fatigue loading	γ_{m5}
- loading basically static	1.0
- significant fatigue loading, periodic inspection, good access	1.5
- significant fatigue loading, periodic inspection, poor access	2.0
- significant fatigue loading, no inspection/maintenance	2.5

If the same system is to be used for strengthening of an actual member, the experimentally determined characteristic stress can be compared to the bond stress calculated for the strengthened beam. For the strengthened beam, the first step is to determine the shear stress distribution along the length of the strip starting from its end. This analysis is based on the elastic modulus and moment of inertia of both the beam and the strip, the geometric configuration of the strengthened beam, the thickness of the adhesive, and the material properties of the adhesive. Similarly, the normal stresses can also be considered using a similar procedure to ensure that the maximum principal bond stress is lower than the characteristic stress determined empirically.

5.3 Design Procedure

Determination of the bond stresses can be completed analytically using the equations given in Schnerch (2005). The equations were established by considering differential equilibrium of a section of the strengthened beam and

applying the principles of compatibility while allowing shear deformations of the adhesive layer. The solutions to the governing differential equations for both the shear and normal stresses are presented for the case of four-point bending with the length of the FRP strip longer than the distance between the load points as shown in Figure 8. Other loading configurations require re-solution of the governing differential equations and implementation of the appropriate boundary conditions. Using these equations, the distribution of the shear and normal stresses in the adhesive joint can be established along the entire length of the bonded strip. Considering the end of the FRP strip, where the shear and normal stresses in the adhesive are typically the greatest, these equations become:

$$t_{max} = B_1 + m_1 P \qquad \text{Equation (6)}$$

$$s_{max} = C_1 - n_1 B_2 l \qquad \text{Equation (7)}$$

where

$$B_1 = \frac{-G_a}{t_a l}\left[(a_{FRP} - a_s)\Delta T - \frac{y_s}{E_s I_s} Pa\right] - m_1 P e^{-k}$$

$$B_2 = \frac{G_a}{t_a l}\left[(a_{FRP} - a_s)\Delta T - \frac{y_s}{E_s I_s} Pa\right]$$

$$C_1 = \frac{E_a P}{2b^3 t_a E_s I_s}(1 + ba) - \frac{n_3}{2b^3} t_{max} + \frac{n_1}{2b^3}\left(B_1 l^4 + b^3 B_2 l^3\right)$$

$$k = l(b - a)$$

$$m_1 = \frac{G_a}{t_a l^2}\left(\frac{y_s + y_{FRP}}{E_s I_s + E_{FRP} I_{FRP}}\right)$$

$$n_1 = \frac{y_s E_{FRP} I_{FRP} - y_{FRP} E_s I_s}{E_s I_s + E_{FRP} I_{FRP}}$$

$$n_3 = \frac{E_a b_{FRP}}{t_a}\left(\frac{y_s}{E_s I_s} - \frac{y_{FRP}}{E_{FRP} I_{FRP}}\right)$$

$$b = \sqrt[4]{\frac{E_a b_{FRP}}{4 t_a}\left(\frac{1}{E_s I_s} + \frac{1}{E_{FRP} I_{FRP}}\right)}$$

$$l^2 = \frac{G_a b_{FRP}}{t_a}\left(\frac{(y_s + y_{FRP})(y_s + y_{FRP} + t_a)}{E_s I_s + E_{FRP} I_{FRP}} + \frac{1}{E_s A_s} + \frac{1}{E_{FRP} A_{FRP}}\right)$$

$A_{FRP,s}$ = cross-sectional area

b_{FRP} = width

$E_{a,FRP,s}$ = tensile elastic modulus

G_a = shear modulus

$I_{FRP,s}$ = moment of inertia

$t_{a,FRP}$ = thickness

$y_{FRP,s}$ = distance from the centroid of the element to the surface in contact with the adhesive

$\alpha_{FRP,s}$ = coefficient of thermal expansion

ΔT = temperature difference

a,b & P are as defined in Figure 8 and the subscripts a, FRP & s refer to the adhesive, FRP and transformed steel-concrete composite beam respectively.

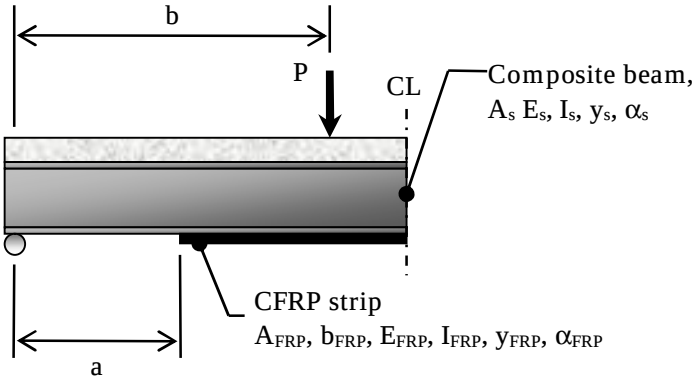

Figure 8 Definition of the variables used to calculate bond stresses

While the above equations are quite involved, they are of a closed form and can be solved relatively easily using commercially available software.

Equations (6) and (7) assume that the ends of the CFRP strips are square without any taper or spew fillet. This represents a worst case scenario resulting in the highest bond stresses. Using finite element analysis, researchers have demonstrated that bond stresses can be reduced by up to 60 percent by

incorporating a reverse taper and a spew fillet at the termination of the CFRP strengthening materials as shown in Figure 3 (Hildebrand, 1994). Due to the resulting geometric discontinuity, the governing differential equations must be solved using a numerical procedure as discussed by Schnerch (2005) and Deng ***et al.*** (2003). However, this technique may be overly cumbersome to be used for design purposes. It is recommended that a conservative approach be taken in the design of the adhesive joint. The design should be based on the assumption of a square termination of the strengthening materials using Equations (6) and (7) above. However, the strengthening should be detailed to reduce the bond stresses by incorporating a reverse taper, a spew fillet and possibly a transverse fiber wrap at all terminal points of all FRP strips whenever possible. Additionally, the ends of the strengthening materials and any necessary splices should be located at locations of low bending moment to further reduce the bond stresses at the end of the joint.

Thus, the adhesive joint should be designed such that

$$\gamma_{m1}\gamma_{m2}\gamma_{m3}\gamma_{m4}\gamma_{m5}\sigma_{p,\,max} \leq \sigma_c \qquad \text{Equation (8)}$$

where γ_{mi} are the material partial factors presented in Table 3, $\sigma_{p,max}$ is the maximum principle stress at the end of the adhesive joint, calculated by substituting Equations (6) and (7) into Equation (5) and σ_c is the characteristic strength of the adhesive determined from representative tests.

6. SPLICE DETAILING

In order to implement a CFRP strengthening system to longer span bridges and structures, it may be necessary to splice finite lengths of the HM strips along the length of the member. To ensure adequate transfer of stresses across the joint, a lap-splice cover plate should be provided as shown schematically in Figure 9. Test results and numerical modeling (Dawood & Rizkalla, 2007) indicate the presence of high bond stress concentrations at the main plate ends and at the ends of the CFRP splice plate. The stress concentrations at these locations can be significantly reduced by providing a reverse tapered plate end detail with an adhesive spew

fillet as shown in Figure 9. In a recent study it was shown that splices with reverse tapered plate end details at all critical locations exhibited at least twice the capacity of similar joints with square plate ends (Dawood & Rizkalla, 2007). The plate ends in this study were tapered to an angle of approximately 20^{o} with a corresponding 20^{o} spew fillet extending beyond the end of the plate as shown schematically in Figure 9. In order to prevent premature debonding of the splice plate due to interaction between the bond stress concentrations at the plate end locations it is recommended to use a splice plate which is at least 800 mm long.

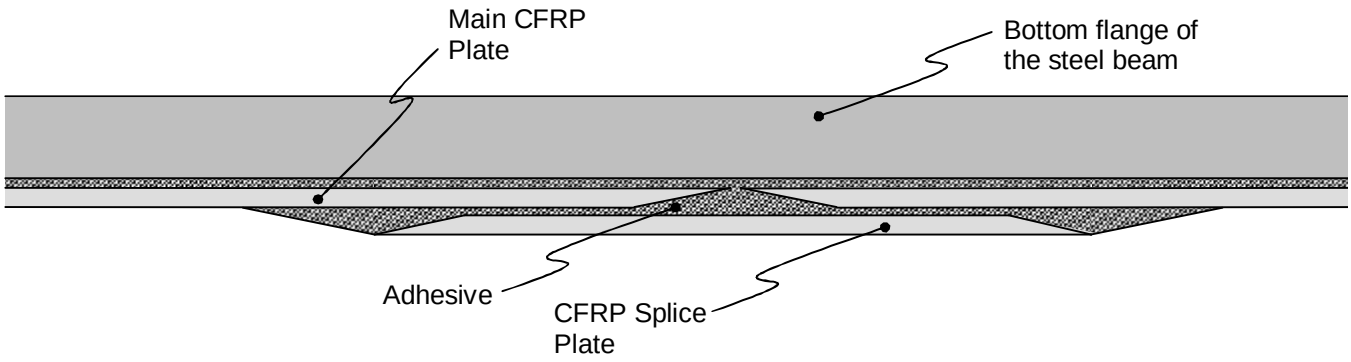

Figure 9 Side view of splice plate detail

Splice joints should be located as close to points of inflection or points of small magnitude of moment as practical. Splices should not be installed at locations of high moment as this may lead to premature failure of the strengthening system due to debonding of the splice plate. The results of an extensive experimental and finite element study indicate that the presence of a splice joint induces a strain concentration in the main CFRP plate near the toe of the splice plate. Test results of an 800 mm long splice plate with reverse tapered plate ends indicate that debonding occurred a t a strain concentration within the main CFRP plate immediately adjacent to the splice plate equivalent to 67 percent of the rupture strain of the CFRP material (Dawood & Rizkalla, 2007). This strain corresponds to a strain, away from the end of the splice plate, of approximately 50 percent of the CFRP rupture strain. Due to the non-linearity of the moment-curvature relationship of the section, the moment corresponding the 50 percent of the

rupture strain is approximately 60 percent of the maximum moment applied to the strengthened beam. Therefore it is recommended to locate the splices where the moment is less than 60 of the maximum applied factored moment. This location is expected to produce a strain in the main plate at the selected splice location equal to or less than 50 percent of the rupture strain of the CFRP.

Appendix – Example Calculations

To demonstrate the application of the design principles described in these guidelines, the analysis of a typical strengthened steel-concrete composite beam was considered. The dimensions of the example beam are given in Figure 10.

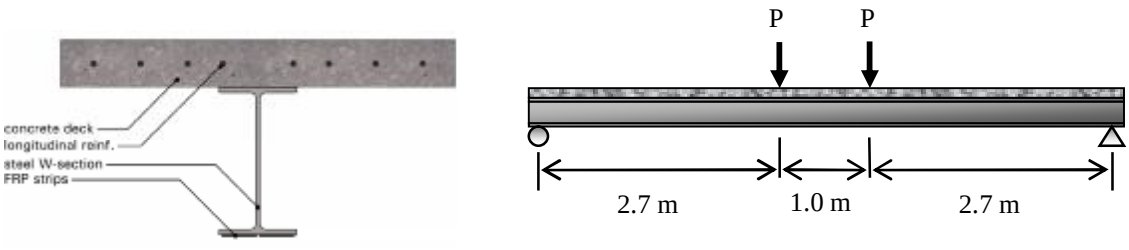

Section **Elevation**

Geometric Properties

Concrete Deck		***FRP Strip***	
Width, w_c	= 840 mm	Width, b_{FRP}	= 150 mm
Thickness, t_c	= 100 mm	Thickness, t_{FRP}	= 4 mm
Longitudinal Reinf.		***Steel W-Section (W310 x 45)***	
Area, A_s	= 1000 mm^2	Width, b	= 165 mm
Distance from top, d_s	= 50 mm	Height, h	= 315 mm
		Flange Thickness, t_f	= 10 mm
		Web thickness, t_w	= 7.0 mm

Figure 10 Dimensions of the example beam

The material properties of the example beam are given in Figure 11. The complete stress-strain relationship of the concrete in the compression zone of the beam is defined in terms of the measured cylinder compressive strength using the expression presented in the figure (Collins and Mitchell, 1997). The constants n, k, ε_c and ε_{cu}, which are presented in Figure 11, were determined to provide a best fit of the measured stress-strain curve for a series of representative concrete cylinders. Alternatively, Collins and Mitchell (1997) provide expressions which can be used to determine these constants if only the compressive strength, f_c' of a representative cylinder is known. An elastic-perfectly plastic material model was used to represent the structural steel W-section and the longitudinal reinforcement as shown in Figure 11. The linear-elastic material model used for the CFRP is also shown in the figure.

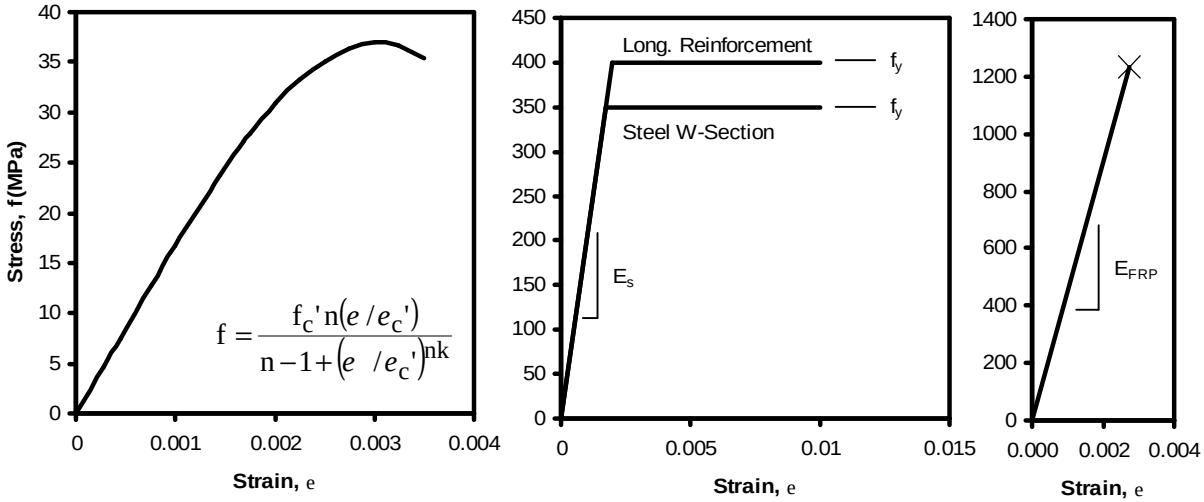

(a) Concrete (*Collins and Mitchell, 1997*)) **(b) Steel** **(c) HM CFRP**

Material Properties

Concrete

Cylinder strength, f_c'	= 37.0 MPa
Strain at peak stress, ε_c'	= 0.0031
Failure strain, ε_{cu}	= 0.0035
Curve fitting factor, n	= 3.27
Post peak factor, k	= 1.00 $\varepsilon_c < \varepsilon_c'$
	= 1.23 $\varepsilon_c > \varepsilon_c'$

Steel W-Section

Modulus of Elasticity, E_s	= 200 GPa
Yield strength, f_y	= 360 MPa

Longitudinal Reinf.

Modulus of Elasticity, E_s	= 200 GPa
Yield strength, f_y	= 400 MPa

FRP Strip

Modulus of Elasticity, E_{FRP}	= 450 GPa
Mean strength, $\bar{f}_{FRP,u}$	= 1543 MPa
Standard deviation, σ	= 30 MPa

Figure 11 Material properties for the example beam

This beam was also tested to failure at NC State University to examine the accuracy and conservativeness of the proposed design guidelines. Details of the example beam test can be found in Schnerch (***2005***). The moment-curvature relationship of the strengthened beam was calculated at the service load level and at the ultimate level based on the proposed design procedure. The moment-curvature relationship was extended to predict the load-deflection behavior of the example beam. Finally, the maximum bond stresses at the ends of the CFRP strip are calculated at the service load level to check the suitability of the adhesive joint.

A.1 Moment-Curvature Relationship

The following sections present detailed calculations of the moment and curvature of the strengthened section under service loading conditions and at ultimate, based on the procedures presented in these guidelines. The predicted nominal moment and curvature are also compared to the measured moment and curvature for the example beam.

A.1.1 Service Loading Conditions

The concrete deck and FRP strips are transformed to equivalent areas of steel and the neutral axis depth, c of the transformed section is calculated as presented in Table 4.

$$w_{c,t} = \frac{E_c}{E_s} w_c = 71.3 \text{ mm}$$

$$w_{FRP,t} = \frac{E_{FRP}}{E_s} w_{FRP} = 337.5 \text{ mm}$$

Table 4 Calculation of the elastic neutral axis depth of the transformed section

Component	Transformed Area, A_t	Distance from top, y	A y
Concrete deck	7,130 mm^2	50 mm	356,500 mm^3
Longitudinal reinf.	1,000 mm^2	50 mm	50,000 mm^3
Steel W-section	5,365 mm^2	257.5 mm	1,381,488 mm^3
FRP strip	1,350 mm^2	417 mm	562,950 mm^3
	$\Sigma A = 14{,}845$ mm^2		$\Sigma Ay = 2{,}350{,}938$ mm^3

$$c = \frac{\sum Ay}{\sum A} = 158 \text{mm}$$

The maximum strain at the tension flange of the steel beam should not exceed $0.6\varepsilon_y$ under service loading conditions. Thus, the curvature of the section is,

$$f = \frac{0.6(0.0018)}{(415 - 158)} = 4.1 \text{x} 10^{-6} \text{ rad/mm}$$

From the known curvature and the strain at the bottom of the steel section, the strain at different levels through the cross-section is determined. The corresponding stresses are calculated using the appropriate material model

recognizing that the materials remain linear under service loading conditions. The strains and stresses are presented in Figure 12 and Table 5.

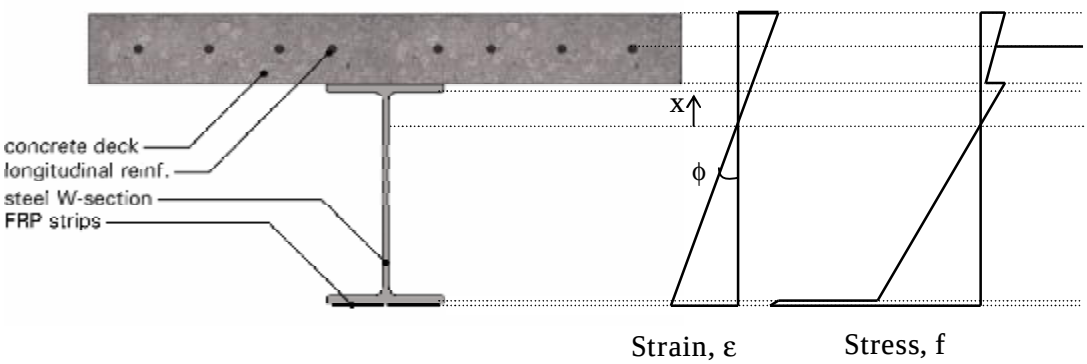

Figure 12 Strain and stress profiles under service loading conditions

Table 5 Strain and stress at different levels under service loading conditions

Level	Strain	Stress
Top of concrete deck	0.67×10^{-3} (C)	11.5 MPa
Longitudinal Reinforcement	0.46×10^{-3} (C)	92 MPa
Bottom of concrete deck	0.25×10^{-3} (C)	4.3 MPa
Top of top flange of steel W-section	0.25×10^{-3} (C)	50 MPa
Bottom of top flange of steel W-section	0.20×10^{-3} (C)	40 MPa
Top of bottom flange of steel W-section	1.01×10^{-3} (T)	202 MPa
Bottom of bottom flange of steel W-section	1.05×10^{-3} (T)	210 MPa
Top of CFRP strip	1.05×10^{-3} (T)	473 MPa
Bottom of CFRP strip	1.06×10^{-3} (T)	477 MPa

The resultant force, corresponding moment arm and moment contribution of each component of the cross-section, can be calculated from the geometry of the section as presented in Table 6.

Table 6 Calculated resultant force, moment arm and moment at different levels through the cross-section under service loading conditions

Component	Resultant force, F	Moment arm, y	Moment, M
Concrete deck	652 kN (C)	118 mm	77 kN-m
Reinforcing steel	91 kN (C)	110 mm	10 kN-m
Steel W-section	457 kN (T)	31.2 mm	126 kN-m
CFRP strip	286 kN (T)	255 mm	73 kN-m
	$\Sigma F = 0$ kN		**ΣM = 286 kN-m**

Under service loading conditions, the moment and curvature of the section are,

$M_s = 286$ kN-m, $\phi_s = 4.1 \times 10^{-6}$ rad / mm

A.1.2 Ultimate Loading Conditions

The nominal moment capacity of the strengthened section was calculated using a similar procedure. The nominal capacity is governed by rupture of the CFRP strips. The design strength of the CFRP and the corresponding ultimate strain can be calculated as follows:

$$f^{*}_{FRP,u} = \bar{f}_{FRP,u} - 3s = 1453 \text{ MPa}$$

$$f_{FRP,u} = C_E f^{*}_{FRP,u} = 1235 \text{ MPa}$$

$$\varepsilon_{FRP,u} = 0.0027$$

By iteration of the neutral axis depth until force equilibrium was satisfied, the neutral axis was found to be 149 mm below the top surface of the concrete deck. The corresponding curvature of the section immediately prior to rupture of the CFRP strips is 10.1×10^{-6} rad/mm.

From the curvature and the strain at the CFRP strips the strain at different levels through the cross section was calculated. The stress distribution was established using the appropriate material models, this time accounting for the non-linearity of the material properties, as presented in Table 7.

Table 7 Strain and stress at different levels through the cross-section under ultimate loading conditions

Level	Strain	Stress
Top of concrete deck	1.50×10^{-3} (C)	24.5 MPa
Longitudinal Reinforcement	1.00×10^{-3} (C)	200 MPa
Bottom of concrete deck	0.49×10^{-3} (C)	8.3 MPa
Top of top flange of steel W-section	0.49×10^{-3} (C)	98 MPa
Bottom of top flange of steel W-section	0.38×10^{-3} (C)	76.0 MPa
Top of bottom flange of steel W-section	2.56×10^{-3} (T)	360 MPa
Bottom of bottom flange of steel W-section	2.67×10^{-3} (T)	360 MPa
Top of CFRP strip	2.67×10^{-3} (T)	1201 MPa
Bottom of CFRP strip	2.70×10^{-3} (T)	1235 MPa

The resultant force is calculated by integration of the strain profile for each component of the cross section. For example, for the concrete deck the force resultant is given by,

$$F_c = \int_{c-t_c}^{c} w_c(x) f_c(x) dx$$

and after substituting the non-linear material characteristics of the concrete,

$$F_c = b_c \int_{c-t_c}^{c} \frac{f_c' n(fx / e_c')}{n - 1 + (fx / e_c')^{nk}} dx$$

This expression is easily evaluated using a spreadsheet and a numerical integration technique such as Simpson's rule. The resultant forces are presented in Table 8.

Table 8 Calculated resultant forces, moment arms and moments at different levels through the cross-section under ultimate loading conditions

Component	Resultant force, F	Moment arm, y	Moment, M
Concrete deck	1407 kN (C)	83.0 mm	150 kN-m
Reinforcing steel	199 kN (C)	93.4 mm	20 kN-m
Steel W-section	879 kN(T)	18.2 mm	242 kN-m
CFRP strip	726 kN (T)	272 mm	194 kN-m
	$\Sigma F = 1$ kN ≈ 0 kN		Σ**M = 606 kN-m**

The corresponding nominal moment and curvature of the section at ultimate loading conditions are,

$M_{n,S} = 606$ kN-m, $\phi_u = 10.1 \times 10^{-6}$ rad / mm

Therefore, the ultimate moment capacity of the strengthened section based on a strength reduction factor, ϕ, of 0.75 is

$M_{U,S} = 455$ kN-m

A.1.3 Comparison with Experimental Results

The experimental results of the beam test indicate that failure of the beam occurred due to rupture of the HM CFRP strips when the strain at the level of the HM CFRP reached the mean rupture strain reported by the manufacturer of 0.0033 (Schnerch, 2005). The corresponding applied moment immediately prior to failure was 663 kN-m. Based on the proposed moment-curvature analysis, the moment capacity of the section corresponding to a strain of 0.0033 at the level of the CFRP strips was calculated as 674 kN-m which correlates well with the measured experimental results. The moment and curvature of the section were also

calculated for several points prior to rupture of the CFRP. The predicted and measured moment-curvature relationships are compared in Figure 13. Inspection of the figure demonstrates that the calculated moment and curvature of the section accurately predict the measured values prior to yielding of the steel. The slight deviation after yielding, which can be seen in the figure, reflects the effect of the residual stresses which form in the steel section during the manufacturing process (Dawood, 2005). Due to the reduction of the design strength of the CFRP materials, the calculated nominal moment capacity of the section is lower than measured nominal capacity. This demonstrates that the proposed procedure is conservative. The calculated ultimate capacity of the section is also presented in the figure for reference purposes.

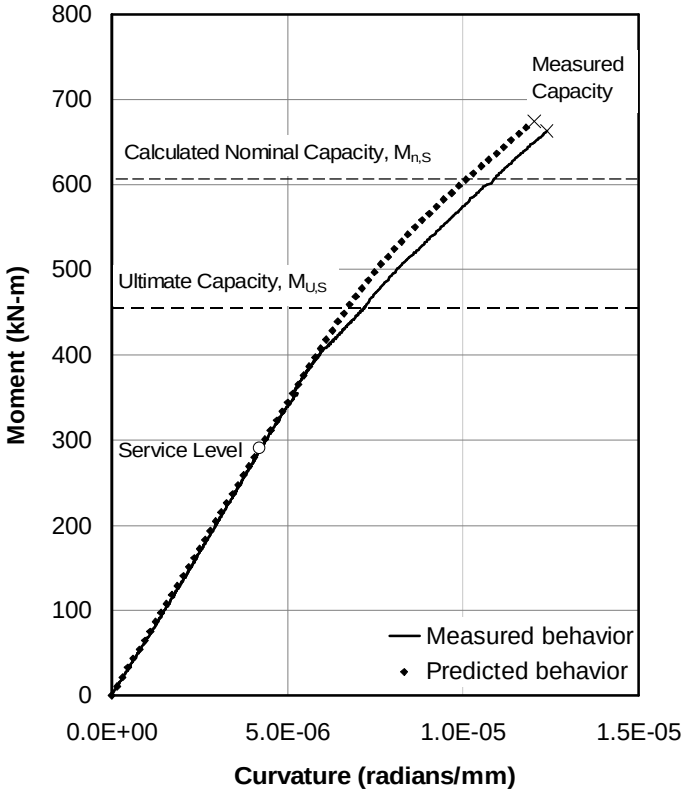

Figure 13 Comparison of the predicted and calculated moment and curvature for the example beam up to rupture of the CFRP

The moment-curvature relationship of the unstrengthened beam was also calculated using a similar analysis procedure, however, neglecting the effect of the

HM CFRP materials. The service moment for the unstrengthened beam, based on 60 percent of the yield moment, was calculated to be 193 kN-m. The nominal moment capacity of the unstrengthened section, $M_{n,US}$, was calculated such that the maximum strain at the top surface of the concrete deck approached the ultimate strain of the concrete, ε_{cu} at failure. The calculated nominal moment capacity was 444 kN-m. The ultimate moment capacity of the section was calculated based on a strength reduction factor, ϕ, of 0.85 as recommended by the AISC LRFD Specification (2001). The increased resistance factor used, as compared to that used for the strengthened section, is justified due to the inherent ductility of the unstrengthened section. The ultimate moment capacity of the unstrengthened section, $M_{U,US}$ was calculated as 377 kN-m.

The moment-curvature relationships of the strengthened and unstrengthened beam are shown in Figure 14. The service moment, $M_D + M_L$, the factored load including the increased live load, $\alpha_D M_D + \alpha_L M_L$, the ultimate capacity of the strengthened beam, $M_{n,S}$, the nominal capacity of the unstrengthened beam, $M_{n,US}$, and the ultimate capacity of the strengthened beam, $M_{U,US}$, are also shown in Figure 14. The factored load was calculated based on the AASHTO (2002) Strength I limit state with live load and dead load factors of 1.75 and 1.25 respectively. The effect of the dead load was assumed to be 50 percent of the calculated service moment of the unstrengthened beam. As seen in Figure 14, the increased service moment for the strengthened beam, calculated using the proposed procedure, satisfies the three conditions discussed previously. Particularly,

$M_D + M_L = 286$ kN-m $= 0.6\ M_{Y,S}$

$\alpha_D M_D + \alpha_L M_L = 452$ kN-m $< M_{U,S} = 455$ kN-m

$M_D + M_L = 286$ kN-m $< M_{n,US} = 444$ kN-m

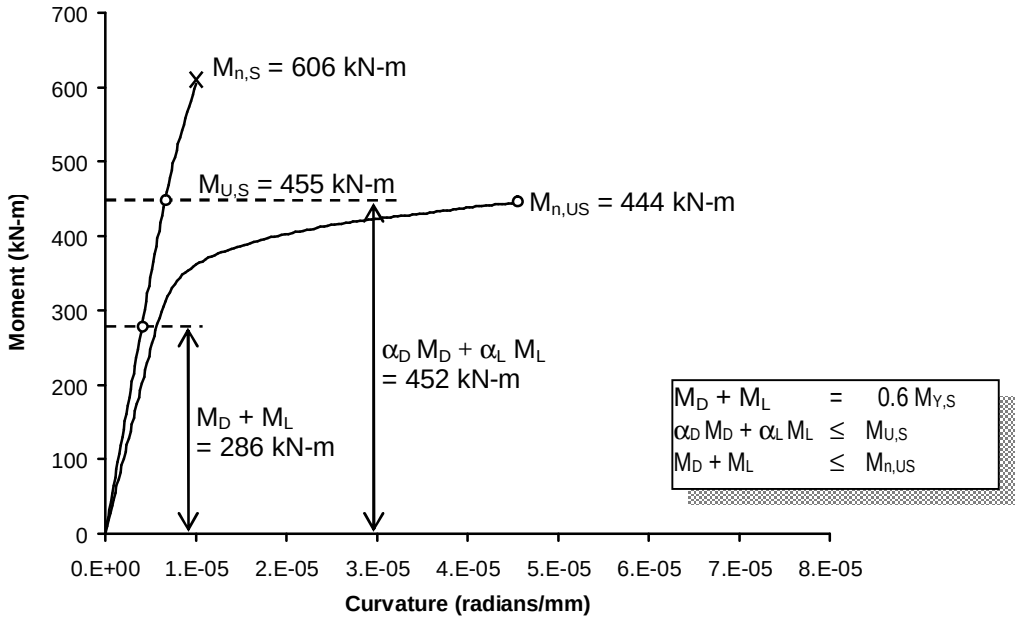

Figure 14 Moment-curvature relationship for the strengthened and unstrengthened beam

The service moment, nominal moment capacity and ultimate moment capacity of the strengthened and unstrengthened beam are summarized in Table 9. The benefit of installing the HM CFRP is evident from the improved performance of the strengthened section as compared to the unstrengthened section.

	Unstrengthened	Strengthened	Increase
Service moment, M_S	193 kN-m	286 kN-m	48%
Nominal moment capacity, M_n	444 kN-m	606 kN-m	36%
Ultimate moment capacity, M_U	377 kN-m	455 kN-m	21%

Table 9 Comparison of the behavior of the unstrengthened and strengthened beam

A.2 Load-Deflection Relationship

The load-deflection response of the example beam was calculated up to design ultimate strain of the CFRP, which corresponds to $P_{n,S}$ of 449 kN, by numerical integration of the curvature of the section for different load levels. The load-deflection behavior of the unstrengthened beam up to crushing of the concrete, which corresponds to $P_{n,US}$ of 332 kN, was also calculated using a similar procedure. The predicted load and deflection of the strengthened and unstrengthened beams are presented in Figure 15. The service load level, $P_D + P_L$,

the factored load including the increased live load, $\alpha_D P_D + \alpha_L P_L$, the nominal capacity of the strengthened beam, $P_{n,S}$, and the nominal capacity of the unstrengthened beam, $P_{n,US}$, are also shown in Figure 15.

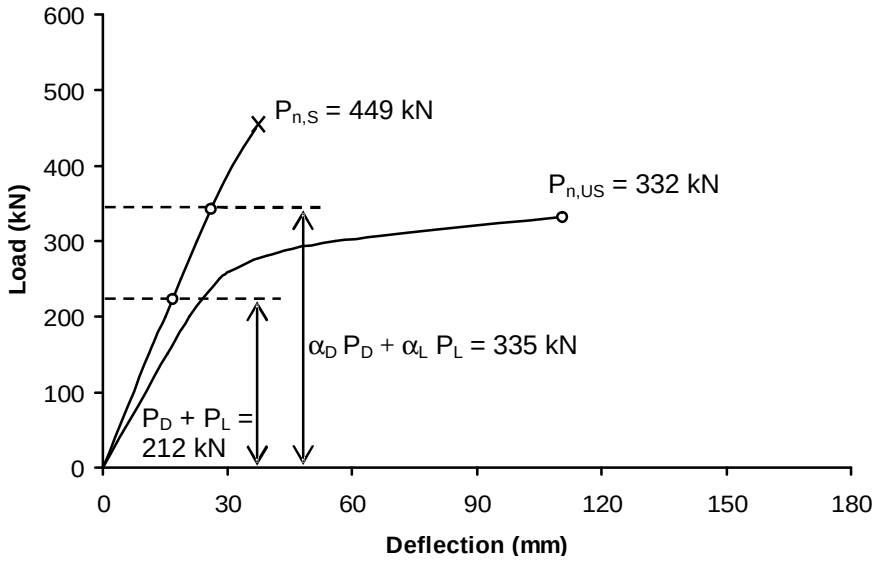

Figure 15 Load-deflection behavior of the example beam

A.3 Bond Stress Analysis

To ensure that debonding will not occur under service loading conditions, it is important to calculate the maximum bond stresses at the end of the adhesive joint. The additional details of the test beam which are needed to calculate the bond stresses are as follows:

Composite beam		***FRP Strip***	
Cross-sectional area, A_s	= 12690 mm^2	Cross-sectional area, A_{FRP}	= 600 mm^2
Moment of Inertia, I_s	= 238.87 x 10^6 mm^4	Moment of Inertia, I_{FRP}	= 800 mm^4
Distance to centroid, y_s	= 281 mm	Distance to centroid, y_{FRP}	= 2 mm
Beam Geometry		***Adhesive***	
Distance from support to end of FRP, a	= 100 mm	Modulus of Elasticity, E_a	= 3000 MPa
		Shear Modulus, G_a	= 1000 MPa
Shear span, b	= 2700 mm	Adhesive thickness, t_a	= 1 mm
		Characteristic strength, σ_c	= 37 MPa*

*based on standard axial tension tests of adhesive coupons

As calculated previously, the total load acting on the strengthened beam at the increased service load level, $P_D + P_L$, is 212 kN. Therefore, for the four-point

bending configuration being considered, the individual point loads are each 106,000 N. Assuming that the temperature of the beam has not changed since the time of installation of the strengthening, and using Equations (6) and (7) the bond stresses are calculated as follows:

λ^2 = 0.867×10^{-3} mm^{-2}
k = 76.56
m_1 = 6.83×10^{-6} mm^{-2}
B_1 = 2.12 MPa
τ_{max} = 2.84 MPa

β = 0.13 mm^{-1}
n_1 = -2.00 mm
n_3 = -2.50×10^{-3} mm^{-3}
B_2 = -2.12 MPa
C_1 = 1.53 MPa
σ_{max} = 1.41 MPa

Applying Equation (5), the maximum principle stress, σ_p, is 3.63 MPa. The appropriate material partial factors can be determined from Table 3 as follows:

γ_{m1}	= 1.25	Given that the characteristic strength of the adhesive was determined from standard tests
γ_{m2}	= 1.25	Given that the adhesive is applied by hand using glass spacer beads to maintain a consistent bond thickness
γ_{m3}	= 1.5	Given that the adhesive may be required to sustain long term loading
γ_{m4}	= 2.0	To account for potential environmental degradation of the adhesive under service conditions which was not accounted for during testing
γ_{m5}	= 2.0	Since bridges are subjected to significant fatigue loading and are typically inspected and maintained on a regular basis, however, access to the tension flange of the main girders may be difficult

Therefore, by applying Equation (8),

$\gamma_{m1}\gamma_{m2}\gamma_{m3}\gamma_{m4}\gamma_{m5}\sigma_{p,max} = 34 \text{ MPa} \leq 37 \text{ MPa} = \sigma_c$

which demonstrates that the bond stresses in the adhesive are sufficiently low to prevent debonding of the strengthening under service loading conditions with a total factor of safety greater than nine. This factor of safety can be further increased by detailing the CFRP strips with a reverse taper, an adhesive fillet and a transverse fiber wrap at each end.

Considering the yield load of the steel beam, of 354 kN, the calculated maximum shear stress, τ_{max}, and normal stress, σ_{max}, in the adhesive joint are 4.75 MPa and 2.35 MPa respectively. The corresponding maximum principle stress, $\sigma_{p,max}$ at the ends of the joint is 6.07 MPa. Therefore, even at yielding of the steel section, the adhesive joint provides a factor of safety of approximately six as compared to the characteristic strength of the adhesive.

A.4 Location of Splice Joints

If material limitations do not allow the use of a continuous plate for the CFRP strengthening system, it may be necessary to splice shorter lengths of the CFRP plates in order to strengthen the entire beam. To ensure optimum performance of the splice joint, an 800 mm long splice plate with reverse-tapered plate ends should be use such as that shown schematically in Figure 9. Based on the proposed guidelines, the splice should be installed at a location where the factored applied moment equal to or less than 60 percent of the maximum value. For the example beam, for a factored applied moment of 452 kN-m, shown in Figure 16, the splice joint should be installed at a location where the applied moment is less than 271 kN-m or less than 1.6 m from the support location as shown in the figure.

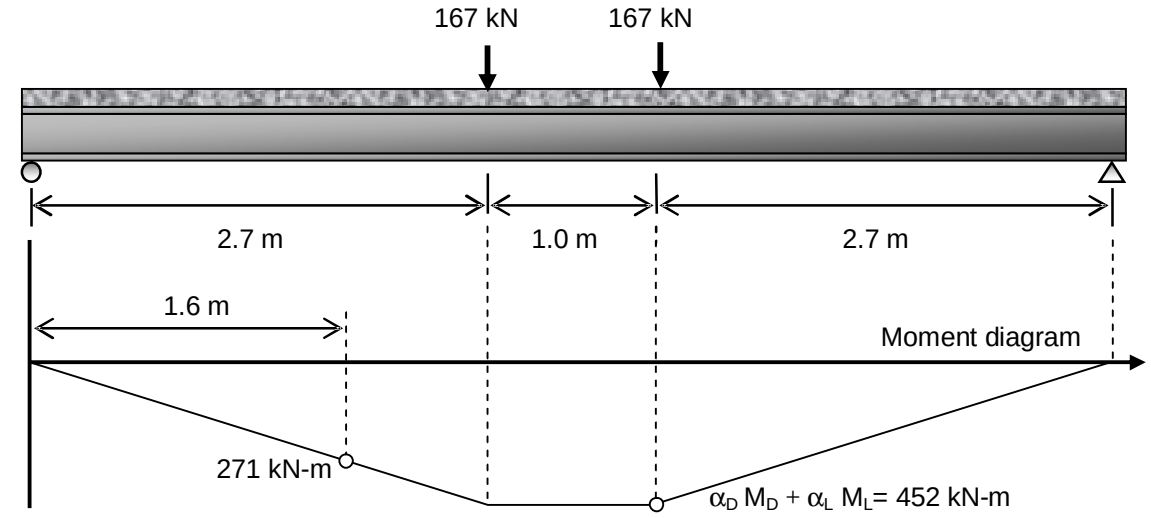

Figure 16 Determination of the location of a splice for the example beam

ACKNOWLEDGEMENTS

The authors would like to acknowledge the support provided by the National Science Foundation (NSF) Industry / University Cooperative Research Center (I / UCRC) for the Repair of Buildings and Bridges with Composites (RB^2C) and the support provided by Mitsubishi Chemical FP America Inc. The significant contributions of Mr. Akira Nakagoshi are acknowledged and thanks are extended for his continual reminder of the needs of the industry.

6. REFERENCES

AASHTO LRFD Bridge Design Specifications. American Association of State Highway and Transportation Officials, Washington D.C., 2002.

AISC Manual of Steel Construction: Load and Resistance Factor Design, Third Edition. American Institute of Steel Construction, Chicago IL, 2001.

Allan, R.C., J. Bird and J.D. Clarke. "Use of adhesives in repair of cracks in ship structures," Materials Science and Technology, v. 4, October 1988, pp. 853-859.

Buyukozturk, Oral, Oguz Gunes, Erdem Karaca. "Progress on understanding debonding problems in reinforced concrete and steel members strengthened using FRP composites," Construction and Building Materials, v. 18, n. 1, February 2004, pp 9-19.

Cadei, J.M.C., T.J. Stratford, L.C. Hollaway, and W.G. Duckett. Strengthening Metallic Structures Using Externally Bonded Fibre-Reinforced Polymers. Publication C595, Construction Industry Research and Information Association (CIRIA), London, UK, 2004, 234 p.

Collins, Michael P.and D. Mitchell. Prestressed Concrete Structures. Response Publications, Canada, 1997.

Dawood, Mina. Fundamental Behavior of Steel-Concrete Composite Beams Strengthened with High Modulus Carbon Fiber Reinforced Polymer (CFRP) Materials. Master's Thesis, North Carolina State University, 2005.

Dawood, Mina and Sami Rizkalla. "Bond and splice behavior of CFRP laminates for strengthening steel beams," Proceedings of the Advanced Composites in Construction Conference – ACIC 07, Bath, United Kingdom, April 2-4, 2007.

Deng, Jun, Marcus M.K. Lee, and Stuart S.J. Moy. "Stress analysis of steel beams reinforced with a bonded CFRP plate," Composite Structures, v. 65, n. 2, August 2004, pp. 205-215.

Francis, R. Bimetallic Corrosion: Guides to Good Practice in Corrosion Control. National Physical Laboratory, Teddington, Middlesex, 2000, 15 p.

Hand, H.M., C.O. Arah, D.K. McNamara, and M.F. Mecklenburg. "Effects of environmental exposure on adhesively bonded joints," International Journal of Adhesion and Adhesives, v. 11, n. 1, January 1991, pp. 15-23.

Hart-Smith, L.J. "Further developments in the design and analysis of adhesive-bonded structural joints," ASTM Special Technical Publication 749, Joining of Composite Materials: A Symposium, K.T. Kedward, ed., April 16, 1980, pp. 3-31.

Hashim, S.A., M.J. Cowling, and I.E. Winkle. "Design and assessment methodologies for adhesively bonded structural connections," International Journal of Adhesion and Adhesives, v. 10, n. 3, July, 1990, pp. 139-145.

Hildebrand, M. "Non-linear analysis and optimization of adhesively bonded single lap joints between fibre-reinforced plastics and metals," International Journal of Adhesives, v. 14, n. 4, 1994, pp. 261-267.

Hollaway, L.C. and J. Cadei. "Progress in the technique of upgrading metallic structures with advanced polymer composites," Progress in Structural Engineering Materials, v. 4,n. 2, April-June, 2002, pp, 131-148.

Hutchinson, A.R. "Surface pretreatment – the key to durability," Proceedings of the International Conference on Structural Faults & Repair, University of London, July 1987, pp. 235-244.

Institution of Structural Engineers. A Guide to the Structural Use of Adhesives. The Institution of Structural Engineers, London, UK, 1999, 51 p.

Mattock, Alan, H. "Flexural strength of prestressed concrete sections by programmable calculator," PCI Journal, January-February, 1979.

Mays, G.C. and A.R. Hutchinson. Adhesives in Civil Engineering. Cambridge University Press, New York, New York, 1992, 333 p.

McKnight, Steven H., Pierre E. Bourban, John W. Gillespie, Jr., and Vistap M. Kharbari. "Surface preparation of steel for surface bonding applications," Infrastructure: New Materials and Methods of Repair, Proceedings of the 3rd Materials Engineering Conference, ASCE, Kim D. Basham, Ed., November 13-16, 1994, San Diego, California, pp. 1148-1155.

Miller, Trent C., Michael J. Chajes, Dennis R. Mertz, and Jason N. Hastings. "Strengthening of a steel bridge girder using CFRP plates," ASCE Journal of Bridge Engineering, v. 6, no. 6, November-December, 2001, pp. 514-522.

Miriyala, S.K., W.C. Tucker, R. Brown, T.J. Rockett. "Mechanism of galvanic blistering in carbon fiber composites," Proceedings of the 9th International Conference on Composite Materials, ICCM/9, Part 5 (of 6), July 12-16, 1993, Madrid, Spain, pp. 546-553.

Parker, B.M. "Adhesive bonding of fibre-reinforced composites," International Journal of Adhesion and Adhesives, v. 14, n. 2, April 1994, pp. 137-143.

Price, A. and R.J. Moulds. "Repair and strengthening of structures using plate bonding," Construction and Building Materials (UK), v. 5, n. 4, December 1991, pp. 189-192.

Schnerch, David and Sami Rizkalla. "Behavior of scaled steel-concrete composite girders and steel monopole towers strengthened with CFRP," Proceedings of The First International Conference on Innovative Materials and Technologies for Construction and Restoration – IMTCR'04, Vol. 1, Lecce, Italy, June 6-9, 2004.

Schnerch, David. Strengthening of Steel Structures with High Modulus Carbon Fiber Reinforced Polymer (CFRP) Materials. Ph. D. Thesis, North Carolina State University, May 2005, 265 p.

Sykes, J.M. "Surface treatments for steel," in Surface Analysis and Pretreatment of Plastics and Metals, D.M. Brewis, Ed., Applied Science Publishers, Ltd., Essex, England, 1982, pp. 153-174.